Water Research 271 (2025) 122880

Contents lists available at ScienceDirect

Water Research

journal homepage: www.elsevier.com/locate/watres

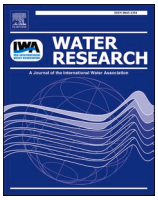

Direct and indirect photolysis of oxolinic acid in surface waters and its inhibition by antioxidant effects

Luca Carena [a,*], Silvia Bertolotti [b,c], Viola Minutoli [a], Mohamed Sarakha [c], Annabel Fernandes [d], Ana Lopes [d], Fabrizio Sordello [a], Marco Minella [a], Davide Vione [a]

[a] Dipartimento di Chimica, Università di Torino, Torino, Italy
[b] Dipartimento di Scienze della Vita e Biologia dei Sistemi, Università di Torino, Torino, Italy
[c] Université Clermont Auvergne, CNRS, Clermont Auvergne INP, ICCF, F-63000 Clermont-Ferrand, France
[d] FibEnTech-UBI, Department of Chemistry, Universidade da Beira Interior, Covilhã, Portugal

ARTICLE INFO

Keywords:
Photochemistry
Contaminants of emerging concern
Dissolved organic matter
Back-reduction
Aquaculture

ABSTRACT

Oxolinic acid is a quinolone antibiotic used in aquaculture to prevent and treat animal diseases. Because of its application and the large expansion of aquaculture in the latest decades, oxolinic acid enters environmental waters through the effluents of aquaculture facilities, posing concerns due to its potential adverse effects on aquatic ecosystems. It is thus important to study the fate of this antibiotic in water bodies. This work investigated the reactivity of the anionic form of oxolinic acid (OxA) by direct and indirect photolysis. The quantum yield of direct photolysis and the bimolecular rate constants of OxA reactions with reactive species photochemically produced in fresh- and seawater (*i.e.*, $HO^{\bullet}$, $CO_3^{\bullet-}$, triplet states of dissolved organic matter, $^1O_2$, and $Br_2^{\bullet-}$) were determined through steady-state irradiation experiments and laser flash photolysis measurements. Results showed that OxA photoreactivity is significant, in particular towards $HO^{\bullet}$ and $CO_3^{\bullet-}$ radicals. However, the direct photolysis and reactions with $CO_3^{\bullet-}$ and the triplet states of dissolved organic matter were found to be significantly inhibited in the presence of phenol, here used as a representative compound for antioxidant dissolved organic matter, most likely because of a back-reduction process.

Photochemical modeling predicted an antibiotic half-life time of some days in fresh- and seawater, showing that OxA degradation is mainly due to direct photolysis in both environments plus reactions with $CO_3^{\bullet-}$ (freshwater) and $Br_2^{\bullet-}$ (seawater).

1. Introduction

Global production of aquatic animals has significantly risen in the last three decades thanks to the huge expansion of aquaculture, which in 2022 surpassed capture fisheries production for the first time (FAO, 2024). Despite dietary and economic benefits for people, aquaculture can negatively impact natural aquatic ecosystems. For instance, intensive farming of aquatic animals often requires veterinary medicinal products, such as antibiotics, to treat and prevent outbreaks of animal diseases (Lulijwa et al., 2020). Although the implementation of treatment processes for fisheries wastewater is currently under way (Ahmad et al., 2021), antibiotics often enter the external environment through the effluents of aquaculture systems, posing several environmental risks (de la Casa-Resino et al., 2021; Zhang et al., 2024).

Oxolinic acid (pK_a ~6.3; Lewis et al., 2016) is a quinolone antibacterial agent used in both fresh- and seawater aquaculture (Samuelsen, 2006). The concentration of this antibiotic in aquaculture water has been reported to range from some tens of μg L^{-1} in aquaculture effluents (Choi et al., 2020) to some hundreds of μg L^{-1} in farming ponds (Le et al., 2005), making the former a potential source of oxolinic acid to the environment. Rigos et al. (2004) have estimated that over 50 kg of oxolinic acid have been released into aquatic environments by Greek fish farms in 2000. Oxolinic acid has been detected at ng L^{-1} levels in both freshwater and seawater around the world (Panthi et al., 2019; Peng et al., 2019; Siedlewicz et al., 2018; Tamtam et al., 2008). Its release into aquatic ecosystems and the associated ecotoxicological risks, such as absorption by wild fauna (Samuelsen et al., 1992) and development of antimicrobial resistance (Shah et al., 2014), warrant investigation into the fate of oxolinic acid in surface waters.

Photodegradation of oxolinic acid plays a major role in its

* Correspondence author at: Dipartimento di Chimica, Università di Torino, Via Pietro Giuria 5, 10125 Torino, Italy.
E-mail address: luca.carena@unito.it (L. Carena).

https://doi.org/10.1016/j.watres.2024.122880
Received 11 September 2024; Received in revised form 13 November 2024; Accepted 27 November 2024
Available online 28 November 2024

attenuation in aquaculture surface pond waters at pH ~8.2 (half-life time = 2–5 days), whereas biodegradation and hydrolysis are almost negligible (Lai and Lin, 2009). Similar results have been reported for seawater (Lunestad et al., 1995; Pouliquen et al., 2007). The photodegradation of a contaminant in sunlit surface waters can take place through direct and indirect photolysis. Direct photolysis occurs when the contaminant absorbs solar light (mainly UV) and undergoes chemical transformation as a consequence; indirect photodegradation involves reactions between the contaminant and Photochemically Produced Reactive Intermediates (PPRIs) (Vione et al., 2014). These PPRIs are transient species which are photoproduced in water bodies upon sunlight absorption by natural-occurring photosensitizers, such as chromophoric dissolved organic matter (CDOM), nitrate and nitrite. Hydroxyl ($HO^{\bullet}$) and carbonate ($CO_3^{\bullet-}$) radicals, singlet oxygen ($^1O_2$), and the excited triplet states of CDOM (^{3}CDOM*) are among the main PPRIs occurring in freshwaters, while the dibromide radical anion ($Br_2^{\bullet-}$) is additionally important in saline waters (Vione et al., 2014).

The photodegradation of contaminants can be inhibited by several natural water components and, most notably, by the dissolved organic matter (DOM). The chromophoric fraction of DOM, CDOM, is the main absorber of photolytic sunlight in surface waters (Nelson and Siegel, 2013), with a resulting light-screening effect that inhibits the direct photodegradation of contaminants. At the same time, indirect photolysis is affected by DOM (not necessarily chromophoric) because of *(i)* effective scavenging of $HO^{\bullet}$, $CO_3^{\bullet-}$, and $Br_2^{\bullet-}$ (Lei et al., 2022; Westerhoff et al., 2007; Wojnárovits et al., 2020) and *(ii)* inhibition of reactions induced by ^{3}CDOM* and $CO_3^{\bullet-}$ by the antioxidant moieties of DOM (Canonica and Laubscher, 2008; Carena et al., 2022; Wenk and Canonica, 2012). Therefore, organic matter acts both as photosensitizer and degradation inhibitor in surface-water photoreactions (Janssen et al., 2014).

Concerning the photodegradation of oxolinic acid in surface waters, little is known about the roles of its direct and indirect photolysis and how these processes are affected by DOM. Louros et al. (2020) reported that, in ultrapure water at pH 7.3, photolysis of oxolinic acid under simulated solar light is reduced by ~60 % after the addition of ~10 $mg_C\ L^{-1}$ DOM, due to light-screening and, possibly, to a role played by the antioxidant moieties of DOM. A similar extent of photolysis inhibition has also been observed in fresh- and brackish water samples with ~8–10 $mg_C\ L^{-1}$ DOM (Louros et al., 2020).

In this work, we investigated the direct and indirect photolysis of the deprotonated form of oxolinic acid (hereafter, OxA), which is relevant to the environmental pH range of surface waters above the pK_a value of the antibiotic. The effect of phenol, chosen as a representative compound for the antioxidant DOM moieties that can inhibit several photodegradation pathways (Wenk and Canonica, 2012), was also studied. The obtained results allowed us to model the photodegradation of OxA in surface waters, estimating both the antibiotic half-life time and the effect of (C)DOM on photodegradation.

2. Materials and methods

2.1. Reagents

A list of the chemicals employed is reported in the Supplementary Material (**Text S1**). All the solutions were prepared with ultrapure water of Milli-Q quality (resistivity 18.2 MΩ cm, TOC < 2 ppb). The desired solution pH was set with phosphate buffer (PB, 2 mM) or, when PB was not used to avoid possible side reactions of phosphate radicals, by 0.1 M NaOH.

2.2. Steady-state irradiation experiments

The direct photolysis of OxA and its reactions with $HO^{\bullet}$, ^{3}CDOM*, and $^1O_2$ were investigated with different steady-state irradiation experiments, consisting of: *(i)* irradiation runs under suitable lamps (to selectively activate processes able to produce the desired PPRIs); *(ii)* quantification of residual OxA over time, and *(iii)* kinetic data fit to determine either quantum yields or reaction rate constants. In general, synthetic aqueous solutions (with, depending on the experiment, volume of 5 or 15 mL, and pH between 8.5 and 10) were irradiated with specific lamps (*vide infra*) inside cylindrical Pyrex glass cells, equipped with a lateral neck tightly closed with a screw cap, and under magnetic stirring. When 5 mL were irradiated, whole solutions were withdrawn from the lamp set-up after scheduled times and analyzed for OxA quantification. In the case of 15 mL solutions, in order not to significantly affect their optical path length (l = 1.2 cm), a maximum of three 1-mL aliquots were sampled from each glass cell to quantify OxA. Depending on the experiment, the following lamps were used to photoproduce the relevant PPRIs and limit secondary reactions effectively: *(i)* a UVB lamp (Philips narrow band TL 20W/01), with emission maximum at 313 nm; *(ii)* a UVA black lamp (Philips TL-D 18 W), with emission maximum at 369 nm; *(iii)* a yellow lamp (Philips TL D 18W/16 Yellow) with emission maximum at 545 nm. The spectral photon flux densities of the UVB and UVA lamps were assessed by chemical actinometry with 2-nitrobenzaldehyde (**Text S2**).

The direct photolysis was studied by irradiating OxA solutions (15 mL, pH 9 by PB) under UVB and under UVA light. A competition kinetics protocol was used to investigate the reactivity between OxA and $HO^{\bullet}$ radical. Different concentrations of the $HO^{\bullet}$-scavenger 2-propanol (iPr; 0–3 mM) were added to the solutions (5 mL, pH 9 by NaOH) containing OxA (23 μM) and $NaNO_3$ (10 mM), the latter used to produce $HO^{\bullet}$ under UVB irradiation (Mack and Bolton, 1999). Reactivity with ^{3}CDOM* was studied by using the excited triplet state of benzophenone-4-carboxylate (^{3}CBBP*) as a surrogate of natural ^{3}CDOM*, because it has been shown that ^{3}CBBP* simulates reasonably well the reactivity of contaminants with ^{3}CDOM* (Carena et al., 2019). In this case, solutions (5 mL, pH 9 by PB) with different OxA concentrations (6–30 μM) were irradiated under UVA light in the presence of CBBP (75 μM). Finally, Rose Bengal (10 μM) was used as $^1O_2$ photosensitizer under yellow light (Ludvíková et al., 2016) to assess OxA reactivity with $^1O_2$ (5 mL solutions, pH 9 by PB).

The possible antioxidant effect of phenol (PhOH) on OxA degradation by direct photolysis and by reactions with ^{3}CDOM* and $CO_3^{\bullet-}$ was also studied with steady-state irradiation experiments. This effect was not assessed in the case of OxA degradation by $HO^{\bullet}$, because the intermediates of $HO^{\bullet}$ reactions are known not to undergo back-reduction by antioxidant compounds (Wenk et al., 2011). In this framework, different PhOH concentrations (0–10 μM) were added to solutions that contained 3 or 6 μM OxA and a photosensitizer if relevant. The experimental conditions details are described in **Text S3**.

Dark controls were performed in parallel to each irradiation run. Solutions with identical chemical composition as those irradiated, but wrapped in a double aluminum foil, were placed under the lamp. It is anticipated that insignificant degradation of OxA was always observed in these conditions.

Quantification of OxA after irradiation was performed by High-Performance Liquid Chromatography coupled with Diode Array Detection (HPLC-DAD). The instrument was a VWR-Hitachi Chromaster equipped with a 5260 autosampler (60 μL injection volume), 5160 quaternary pump, and 5430 DAD detector. The column was a Merck LiChroCART RP-18 cartridge (125 mm × 4 mm × 5 μm), and isocratic elution was carried out with a 53:47 mixture of acidified water (H_3PO_4, pH 2.8) and methanol at a flow rate of 1 mL min^{-1}. The OxA detection wavelength was set at 260 nm.

Time trends of OxA photodegradation were fitted with (pseudo)first-order kinetic equations, determining the rate coefficient (k') for each irradiation run by fitting of experimental data with the equation $[OxA]\cdot[OxA]_0^{-1} = \exp(-k'\cdot t)$, with t as the irradiation time, while [OxA] and $[OxA]_0$ are the concentrations at time t and before irradiation, respectively. The rate of OxA degradation was then calculated as $R_{OxA} = k'\cdot[OxA]_0$.

2.3. Laser flash photolysis experiments

The bimolecular rate constants of OxA with $CO_3^{\bullet-}$, $Br_2^{\bullet-}$ and ^{3}CBBP* were measured through laser flash photolysis (LFP) with a Quanta Ray GCR 130–01 Nd:YAG laser system instrument, used in a right-angle geometry with respect to the monitoring light beam. The apparatus of the instrument includes a detection system, consisting of a pulsed xenon lamp (150 W), a monochromator and a photomultiplier (1P28) that allows for absorbance tracking of the reactive species over time; a spectrophotometer control unit synchronizes the pulsed light source and the programmable shutters with the laser output. A programmable digital oscilloscope (HP54522A) digitizes the signal coming from the photomultiplier and a 32-bit RISC-processor kinetic spectrometer workstation is used to analyze it (Brigante et al., 2010).

The experiments with $CO_3^{\bullet-}$ and $Br_2^{\bullet-}$ were carried out using the fourth harmonic (266 nm) of the laser and an energy of ~40 mJ/pulse. The radical $CO_3^{\bullet-}$ was produced by laser irradiation of 0.03 M H_2O_2 + 0.3 M Na_2CO_3, while $Br_2^{\bullet-}$ was produced by laser irradiation of 0.03 M H_2O_2 + 0.03 M NaBr, in both cases at pH 9. The adopted concentrations of carbonate and bromide ensured that a negligible fraction of $HO^\bullet$ (<2 %) reacted with OxA in these experiments. The measurements with ^{3}CBBP* were performed by using the third laser harmonic (355 nm) and with solutions containing 100 μM CBBP under Ar bubbling, to prevent triplet deactivation by O_2. The decays of $CO_3^{\bullet-}$, $Br_2^{\bullet-}$, and ^{3}CBBP* were monitored at 600 nm, 360 nm, and 540 nm, respectively. Solutions (3 mL) containing the relevant photosensitizers and different OxA concentrations were exposed to a maximum of three consecutive laser shots in a quartz cuvette with a path length of 1 cm. The measured pseudo-first-order decay coefficients of the PPRIs (k', s^{-1}; average of the three consecutive laser pulses) were plotted as a function of [OxA], and the slope of the linear correlation yielded the value of the second-order rate constant.

2.4. Photochemical modeling

The photodegradation of OxA in fresh- and seawater was modeled with the APEX software (Bodrato and Vione, 2014), using the bimolecular rate constants of OxA reactions with $HO^\bullet$, ^{3}CBBP*, $CO_3^{\bullet-}$, $^1O_2$, and $Br_2^{\bullet-}$, as well as its absorption spectrum and quantum yield of direct photolysis. APEX also needs environmental data about water depth and

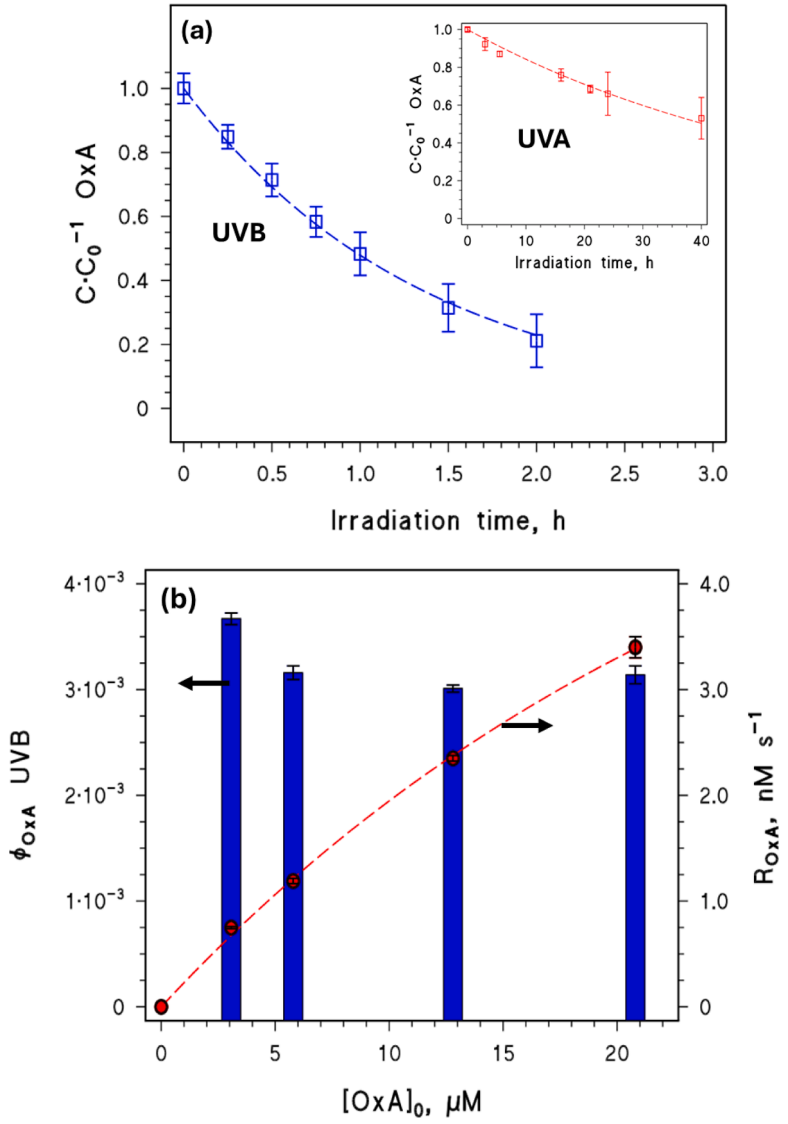

Fig. 1. (a) Observed photodegradation of OxA (6 μM) under UVB and (inset) UVA irradiation at pH 9. The error bounds represent the standard errors of duplicate experiments. **(b)** *Left y-axis*: the blue bars refer to the direct photolysis quantum yields determined under UVB light at different initial concentrations of OxA. *Right y-axis*: measured rates of OxA direct photolysis (red dots) and their interpolation with an equation that describes a light absorption-saturation regime ($R_{OxA} = a \cdot \{1–10^{-b \cdot [OxA]}\}$, dashed red line).

chemical composition (**Table S2**).

APEX gives as output the half-life times and photodegradation rate coefficients of contaminants, referred to a clear-sky scenario corresponding to the 15th of July at 45°N latitude (total UV dose of 7.9×10^5 J m^{-2}; Bodrato and Vione, 2014).

3. Results and discussion

3.1. Direct photolysis

The quantum yield of OxA direct photolysis was determined under UVB and under UVA light. Fig. 1a shows the observed time trends of 6 μM OxA photodegradation, with transformation rates $R_{OxA} = (1.19 \pm 0.06)\cdot10^{-9}$ M s^{-1} under UVB light and $R_{OxA} = (2.25 \pm 0.10)\cdot10^{-11}$ M s^{-1} under UVA. The rates of OxA light absorption in both conditions were calculated as $P_{a,OxA} = \Sigma_i\, p^0(\lambda_i)\cdot[1 - 10^{-A_{OxA}(\lambda i)}]\Delta\lambda$, where $p^\circ(\lambda_i)$ is the spectral photon flux density of the lamp as determined by chemical actinometry (**Text S2**), $A_{OxA}(\lambda_i)$ is the Lambert-Beer absorbance of 6 μM OxA at the wavelength λ_i (see **Fig.S2** for the absorption spectrum of OxA) and $\Delta\lambda = 1$ nm. In particular, it was $P_{a,OxA} = 3.75\cdot10^{-7}$ M s^{-1} under UVB and $P_{a,OxA} = 1.15\cdot10^{-8}$ M s^{-1} under UVA radiation. The quantum yield was determined as $\Phi_{OxA} = R_{OxA}\cdot(P_{a,OxA})^{-1}$, obtaining $\Phi_{OxA} = (3.16 \pm 0.10)\cdot10^{-3}$ for UVB and $\Phi_{OxA} = (1.96 \pm 0.08)\cdot10^{-3}$ for UVA. This variation of OxA quantum yield with wavelength is significantly less marked than that observed for other contaminants (Bhat et al., 2023).

Some contaminants are known to undergo self-sensitized photolysis (*i.e.*, a contaminant photoproduces reactive species that, in turn, react with the contaminant itself) (Hopanna et al., 2020; Zhang et al., 2019), in which case the direct photolysis quantum yield increases with concentration (Bedini et al., 2012). Therefore, the trend of $\Phi_{OxA,UVB}$ *vs.* $[OxA]_0$ was assessed and, as shown in Fig. 1b, there was no significant variation between 3 and 21 μM OxA, with average $\Phi_{OxA,UVB} = (3.3 \pm 0.3)\cdot10^{-3}$. The same figure also shows that the trend of R_{OxA} *vs.* $[OxA]_0$ is mainly accounted for by a light absorption-saturation regime that produces a less-than-linear increase of the rate with increasing substrate concentration, which excludes self-sensitized photolysis (Xie et al., 2016).

3.2. Reactivity of OxA with photoproduced reactive species

Hydroxyl radical. The reaction between OxA and HO$^\bullet$ was studied with nitrate under UVB irradiation. The addition of different concentrations of 2-propanol (iPr) to the relevant solutions caused a significant inhibition of OxA photodegradation (**Fig.S3a**). Since iPr is an efficient HO$^\bullet$ scavenger (Buxton et al., 1988), this inhibition is due to kinetic competition between OxA and iPr for reaction with HO$^\bullet$ (see reactions R.1-R.3). The trend of R_{OxA} *vs.* [iPr] is shown in Fig. 2a. (Buxton et al., 1988)

$$NO_3^- \xrightarrow{h\nu,\ H^+} {}^\bullet NO_2 + HO^\bullet \quad \text{(R.1)}$$

$$HO^\bullet + OxA \rightarrow \text{Products} \qquad k_{HO^\bullet+OxA} \quad \text{(R.2)}$$

$$HO^\bullet + iPr \rightarrow \text{Products} \qquad k_{HO^\bullet+iPr} = 1.9\cdot10^9\ M^{-1}\ s^{-1} \quad \text{(R.3)}$$

$$OxA \xrightarrow{h\nu} \text{Products} \quad \text{(R.4)}$$

By considering the previous reactions and by reasonably applying the steady-state approximation to HO$^\bullet$ concentration, R_{OxA} can be expressed as a function of the initial OxA concentration (Eq. (1)).

$$R_{OxA} = R_{f,HO^\bullet}\frac{k_{HO^\bullet+OxA}[OxA]_0}{k_{HO^\bullet+OxA}[OxA]_0 + k_{HO^\bullet+iPr}[iPr]} + R_{add} \quad (1)$$

In Eq. (1), $R_{f,HO\cdot}$ is the formation rate of HO$^\bullet$ radicals as per reaction R.1, while $k_{HO\cdot+OxA}$ and $k_{HO\cdot+iPr}$ are the bimolecular rate constants of, respectively, R.2 and R.3. The parameter R_{add} is the rate of OxA degradation accounted for by additional pathways, such as the direct photolysis (R.4). Eq. (1) (fitting curve in Fig. 2a) described well the experimental data of R_{OxA} *vs.* [iPr]; the numerical fit yielded $k_{HO\cdot+OxA} = (9.2 \pm 3.0)\cdot10^9$ M^{-1} s^{-1}, $R_{f,HO\cdot} = (1.7 \pm 0.2)\cdot10^{-9}$ M s^{-1} and $R_{add} = (9.9 \pm 1.4)\cdot10^{-10}$ M s^{-1}. The value of $k_{HO\cdot+OxA}$ obtained at pH 9 is reasonably close to that reported at neutral pH ($4\cdot10^9$ M^{-1} s^{-1}) by Zeghioud et al. (2019).

Excited triplet states. As previously mentioned, ^{3}CBBP* was used as ^{3}CDOM* surrogate. In the presence of CBBP and UVA light, the rate of triplet-sensitized OxA degradation was determined as $R_{OxA} = 0.91\cdot k'\cdot[OxA]_0$. In the previous equation k' is the measured pseudo-first-order rate coefficient for OxA phototransformation in the presence of

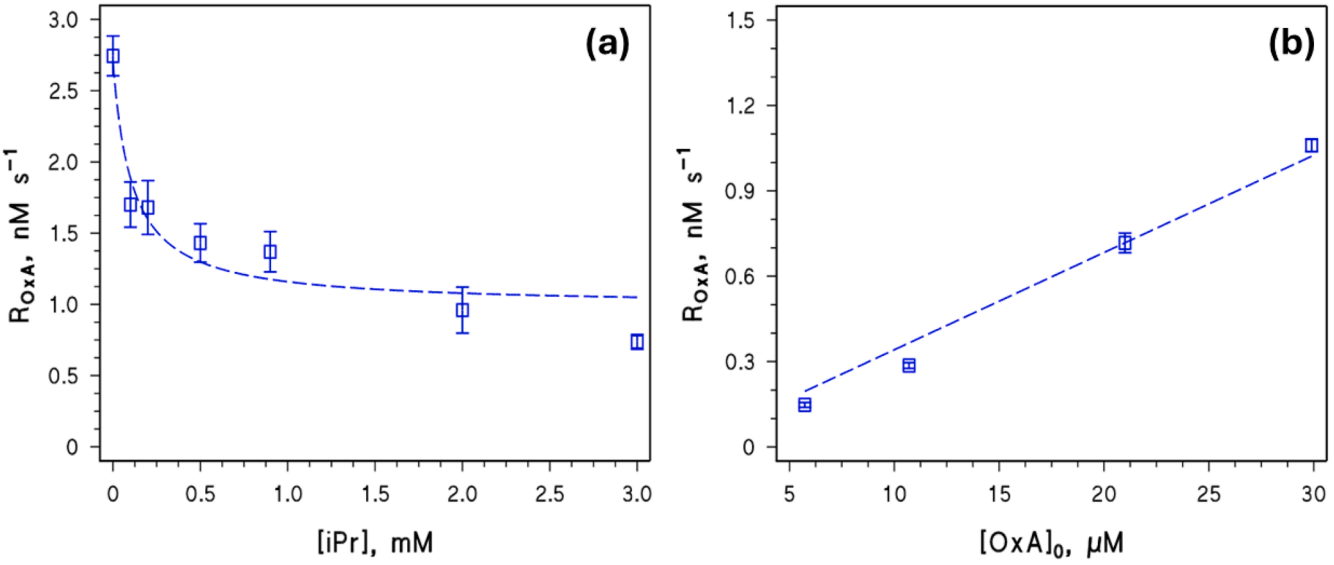

Fig. 2. (a) Rate of OxA photodegradation in the presence of nitrate under UVB light, as a function of added iPr concentration (pH 9). **(b)** Rate of OxA photodegradation in the presence of CBBP under UVA light, as a function of the initial OxA concentration (pH 9). For both figures, open squares are the experimental data with associated standard error, while the dashed curves/lines represent the numerical fit with Eq. (1) (left) or a linear fit (right, least-squares line).

CBBP, while the factor 0.91 takes into account the contribution by OxA direct photolysis to the overall photodegradation. The direct photolysis fraction was in fact determined as ~9 %, from the ratio between the photodegradation rate of OxA measured in the absence of CBBP (direct photolysis) and that observed in the presence of CBBP (direct photolysis + triplet sensitization) (**Fig.S3b)**. Note that the light-screening effect of CBBP on OxA direct photolysis was negligible. It was observed a linear trend between R_{OxA} and $[OxA]_0$ (k' about constant when varying $[OxA]_0$, Fig. 2b), which allowed for the application of a validated protocol to determine the bimolecular rate constant of the reaction between OxA and ^{3}CBBP* ($k_{^3CBBP^*+OxA}$), based on Eq. (2) (Carena et al., 2019) where $k'_d = 6{\cdot}10^5\ s^{-1}$ is the rate constant of ^{3}CBBP* inactivation in aerated solution (Minella et al., 2018), $m = (3.4 \pm 0.2){\cdot}10^{-5}\ s^{-1}$ is the slope of the fit line (R_{OxA} *vs.* $[OxA]_0$, Fig. 2b), while $P_{a,CBBP} = 1.4{\cdot}10^{-8}$ M s^{-1} is the photon flux absorbed by CBBP.

$$k_{^3CBBP^*+OxA} = k'_d \left(\frac{m}{P_{a,CBBP}} - 1.25{\cdot}10^{-6}\ k_{^1O_2+OxA} \right) \quad (2)$$

It should be noted that Eq. (2) includes the contribution of the possible reaction between OxA and $^1O_2$, with bimolecular rate constant $k_{^1O_2+OxA}$. Actually, in the irradiated solutions, $^1O_2$ is produced by the interaction between ^{3}CBBP* and O_2 (Minella et al., 2018) and can potentially react with OxA thereby contributing to its degradation. However, experiments carried out with Rose Bengal as $^1O_2$ photosensitizer (24-h irradiation, yellow light) showed that OxA would not react significantly with $^1O_2$ (**Fig.S3c**). Therefore, $m{\cdot}(P_{a,CBBP})^{-1} - 1.25{\cdot}10^{-6}{\cdot}k_{^1O_2+OxA} \sim m{\cdot}(P_{a,CBBP})^{-1}$, eventually providing $k_{^3CBBP^*+OxA} = (1.5 \pm 0.7){\cdot}10^9\ M^{-1}\ s^{-1}$.

The value of $k_{^3CBBP^*+OxA}$ was also determined with laser flash photolysis (LFP) (**Fig.S4a**) as $(4.8 \pm 0.4){\cdot}10^9\ M^{-1}\ s^{-1}$, which is higher than that found with steady-state irradiation experiments. However, this difference does not look important if one considers that rate constants measured by LFP are sometimes accounted for by both chemical and physical quenching of triplet states (Das et al., 1981), thus a variability within a factor of three is quite common among rate constants of PPRIs reactions determined with different experimental methods (Wojnárovits et al., 2020). Therefore, $k_{^3CBBP^*+OxA} = (1.5 \pm 0.7){\cdot}10^9\ M^{-1}\ s^{-1}$ looks suitable to describe the chemical reactivity of OxA with ^{3}CDOM*. Note that $k_{^3CBBP^*+OxA}$ is within the estimated upper limit of rate constants of ^{3}CDOM* reactions with water contaminants (~$5.9{\cdot}10^9\ M^{-1}\ s^{-1}$; Canonica et al., 2000), and that the excited triplet states of aromatic ketones, including ^{3}CBBP*, are representative of the ^{3}CDOM* pool (Zhou et al., 2019).

Carbonate and dibromide radical anions. Second-order rate constants of OxA reactions with $CO_3^{\bullet-}$ and $Br_2^{\bullet-}$ were determined by LFP (**Fig.S4**). A steady-state irradiation approach could not be used in this case, because of interference by OxA direct photolysis in the systems $NO_3^-/HCO_3^-/CO_3^{2-}$/UVB, $H_2O_2/HCO_3^-/CO_3^{2-}$/UVB, NO_3^-/Br^-/UVB, and H_2O_2/Br^-/UVB that could be used to produce $CO_3^{\bullet-}$ and $Br_2^{\bullet-}$ upon oxidation by $HO^\bullet$ of, respectively, HCO_3^-/CO_3^{2-} and Br^-. In the case of LFP, the decay of $CO_3^{\bullet-}$ and $Br_2^{\bullet-}$ is directly monitored and, in the absence of spectral interferences, the direct photolysis of OxA is not an issue.

The second-order rate constants obtained by LFP were $k_{CO_3^{\bullet-}+OxA} = (1.3 \pm 0.3){\cdot}10^{10}\ M^{-1}\ s^{-1}$ and $k_{Br_2^{\bullet-}+OxA} = (1.4 \pm 0.1){\cdot}10^9\ M^{-1}\ s^{-1}$, showing high reactivity of OxA with $CO_3^{\bullet-}$ and $Br_2^{\bullet-}$. Interestingly, both $CO_3^{\bullet-}$ and $Br_2^{\bullet-}$ react mainly through electron transfer (Lei et al., 2021; Wojnárovits et al., 2020).

3.3. Effect of phenol on OxA degradation induced by ^{3}CBBP*, $CO_3^{\bullet-}$, and the direct photolysis

Phenol has been widely used as a reference compound/competitor in lab experiments aimed at determining the reactivity of water contaminants with PPRIs. It is also a representative compound for the antioxidant (mostly phenolic) moieties of DOM, due to its molecular structure, reactivity, and oxidation properties (Guo et al., 2021; Huang and Zhang, 2022; Wenk and Canonica, 2012; Yan et al., 2019). Moreover, PhOH does not absorb either UVB or UVA light, thereby preventing any light-screening effect on the investigated photoreactions and any side reactions.

Degradation induced by ^{3}CBBP*. Under UVA light and in the presence of CBBP, the observed OxA photodegradation at pH 8.5 is triggered by ^{3}CBBP* with rate constant $k_{^3CBBP^*+OxA}$. The addition of PhOH in the 0.5–10 μM concentration range caused considerable inhibition of OxA degradation, up to ~93 % at 10 μM PhOH (**Fig.S5a**).

Phenol reacts with ^{3}CBBP* with rate constant $k_{^3CBBP^*+PhOH} = 8.9{\cdot}10^8\ M^{-1}\ s^{-1}$ (Minella et al., 2018), thereby potentially subtracting ^{3}CBBP* from reaction with OxA. However, ^{3}CBBP* decays in aerated solution with rate constant $k'_d = 6{\cdot}10^5\ s^{-1}$ and PhOH does not affect ^{3}CBBP* photoproduction as it does not screen UVA light. Therefore, 10 μM PhOH could only induce a ~1.5 % decrease in the steady-state [^{3}CBBP*] by reacting with ^{3}CBBP*. Consequently, PhOH could only decrease by ~1.5 % the degradation rate of OxA induced by ^{3}CBBP*, which cannot possibly account for the observed ~93 % inhibition ($R_{OxA} \sim 0.07{\cdot}R^0_{OxA}$, where R_{OxA} is the rate of OxA decay in the presence of 10 μM phenol and R^0_{OxA} is the decay rate without phenol). Thus, most of the PhOH effect should be accounted for by a typical antioxidant scenario (Canonica and Laubscher, 2008).

Fig. 3a shows the trend of the ratio $R_{OxA}{\cdot}(R^0_{OxA})^{-1}$ as function of the added PhOH concentration, which is well described by a general back-reduction kinetic model (Canonica and Laubscher, 2008). Such a model considers *(i)* OxA photodegradation by ^{3}CBBP* to produce a partially oxidized intermediate, $OxA^{\bullet+}$, and further possible OxA products (R.5); *(ii)* evolution of $OxA^{\bullet+}$ towards final products (R.6), and *(iii)* reduction of $OxA^{\bullet+}$ back to OxA induced by PhOH, which acts as an antioxidant (R.7).

$$OxA \xrightarrow{^3CBBP^*} OxA^{\bullet+} + \text{further products} \qquad k_{^3CBBP^*+OxA} \quad (R.5)$$

$$OxA^{\bullet+} \rightarrow \text{products} \qquad k'_{OxA^{\bullet+}} \quad (R.6)$$

$$OxA^{\bullet+} + PhOH \rightarrow OxA + PhO^\bullet + H^+ \qquad k_{OxA^{\bullet+}+PhOH} \quad (R.7)$$

The experimental data of $R_{OxA}{\cdot}(R^0_{OxA})^{-1}$ *vs.* [PhOH] were interpolated with Eq. (3) (Wenk and Canonica, 2012), where $[PhOH]_{1/2}$ is defined as the phenol concentration that halves the rate of OxA photodegradation measured in the absence of PhOH (reactions R.5, R.6). It has been shown that $[PhOH]_{1/2} = k'_{OxA^{\bullet+}}{\cdot}(k_{OxA^{\bullet+}+PhOH})^{-1}$ (Wenk et al., 2011). Therefore, the lower is $[PhOH]_{1/2}$, the stronger is the inhibition by back-reduction. In this case, we found $[PhOH]_{1/2} = (0.50 \pm 0.10)$ μM.

$$\frac{R_{OxA}}{R^0_{OxA}} = \frac{f}{1 + \frac{[PhOH]}{[PhOH]_{1/2}}} + (1 - f) \quad (3)$$

The parameter f refers to the fraction of OxA that is oxidized by ^{3}CBBP* to $OxA^{\bullet+}$, while $1 - f$ refers to the fraction of OxA that produces different compounds, which do not undergo back-reduction through R.7. In our case, the numerical fit of the experimental data with Eq. (3) yielded $f = 0.99 \pm 0.01$, suggesting that production of intermediates undergoing back-reduction is the main OxA transformation pathway upon reaction with ^{3}CBBP* ($f \sim 1$ and $1 - f \sim 0$).

The back-reduction by phenolic antioxidants occurring in DOM can inhibit the triplet-sensitized degradation (started by electron transfer to ^{3}CDOM*) of electron-rich molecules such as anilines (Canonica and Laubscher, 2008; Leresche et al., 2020). Interestingly, the value of $[PhOH]_{1/2}$ obtained for OxA is lower than that of other water contaminants, thereby suggesting that DOM phenolic moieties have the potential to considerably inhibit the ^{3}CDOM*-sensitized degradation of OxA in surface waters.

Degradation induced by $CO_3^{\bullet-}$. The effect of PhOH on OxA

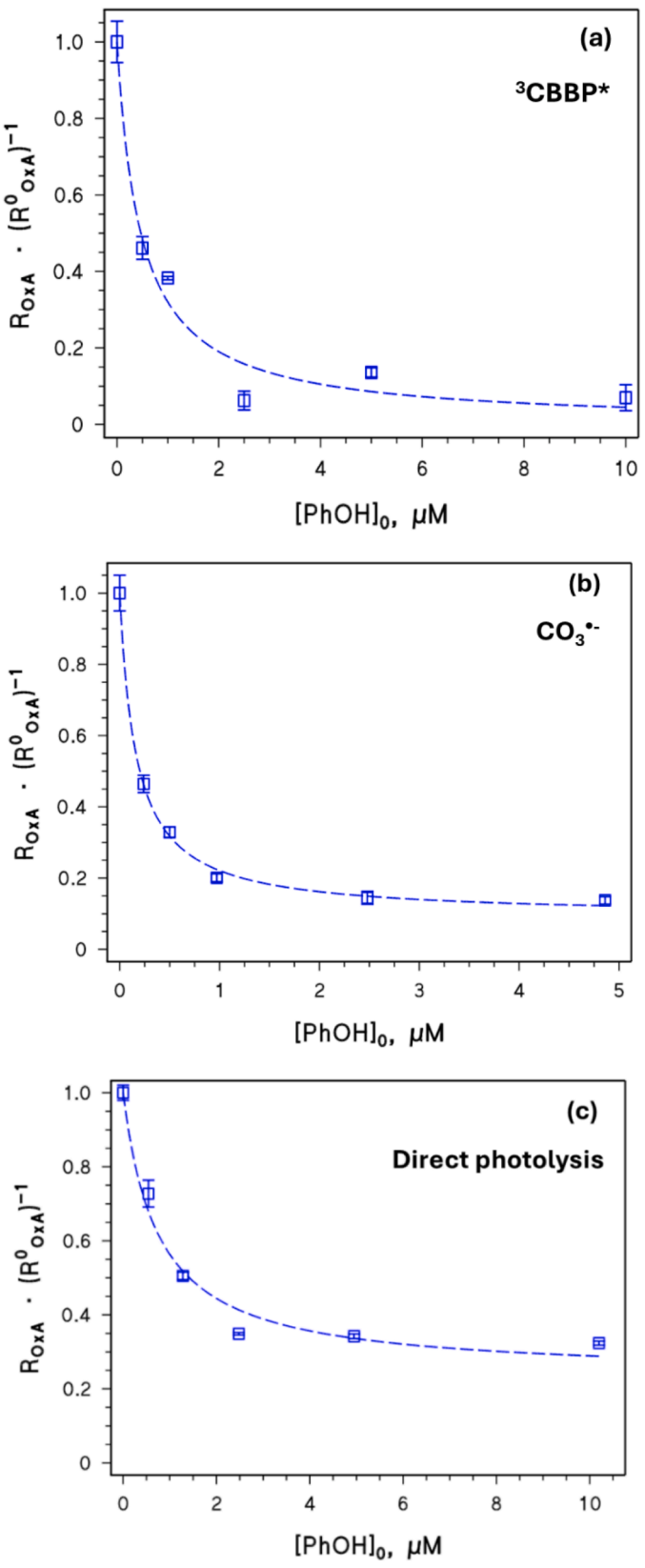

Fig. 3. Inhibition effect of phenol (PhOH) on OxA degradation induced by **(a)** reactions with ^{3}CBBP*, **(b)** reactions with $CO_3^{\bullet-}$, and **(c)** the direct photolysis. Open blue squares with error bars are experimental data with associated standard error, while the dotted blue lines represent the numerical fit with Eq. (3).

degradation induced by $CO_3^{\bullet-}$ was investigated by UVA irradiation of solutions containing CBBP (70 μM), OxA (3 μM), a carbonate buffer (0.5 M $NaHCO_3$ + 0.15 M Na_2CO_3) at pH 10, and variable concentrations of PhOH (0–5 μM). The chosen experimental conditions allowed us: *(i)* to produce ^{3}CBBP* upon light absorption by CBBP; *(ii)* to maximize the amount of ^{3}CBBP* that oxidized carbonate to $CO_3^{\bullet-}$ (R.8), with negligible roles by other reactions of ^{3}CBBP* chemical quenching, and *(iii)* to ensure that $CO_3^{\bullet-}$ reacted predominantly with OxA rather than with PhOH and CBBP (**Text S3**).

$$CO_3^{2-} + {}^3\text{CBBP}^* \rightarrow CO_3^{\bullet-} + \text{CBBP}^{\bullet-} \quad \text{(R.8)}$$

$$\text{OxA} \xrightarrow{CO_3^{\bullet-}} \text{OxA}^{\bullet+} + \text{further products} \quad \text{(R.9)}$$

The addition of PhOH inhibited the photodegradation of OxA (Fig. 3b) which was carried out predominantly by $CO_3^{\bullet-}$, while the contribution of ^{3}CBBP* was negligible (**Fig.S5b**). In particular, the degradation rate (R_{OxA}) observed in the presence of 2.5 and 5 μM PhOH was ~14 % of the rate measured without PhOH (R^0_{OxA}). Such an inhibition effect would be accounted for by back-reduction of $OxA^{\bullet+}$ to the original OxA by PhOH (R.7), because the experimental conditions were chosen to minimize scavenging of either ^{3}CBBP* or $CO_3^{\bullet-}$ by PhOH (**Text S3**), and PhOH would also not be able to inhibit the absorption of UVA radiation by CBBP.

Similarly to the case of ^{3}CBBP*, the effect of PhOH on OxA degradation by $CO_3^{\bullet-}$ can be described by a back-reduction model (Wenk and Canonica, 2012) that considers OxA oxidation to $OxA^{\bullet+}$ (and further compounds, *vide infra*) by $CO_3^{\bullet-}$ (R.9), followed by $OxA^{\bullet+}$ evolution through reactions R.6 (further oxidation) and R.7 (back reduction). The numerical fit of the experimental data with Eq. (3) yielded $[\text{PhOH}]_{1/2} = (0.16 \pm 0.02)$ μM and $f = 0.91 \pm 0.01$. In this case, the parameter f can account for the plateau observed for $R_{OxA} \cdot (R^0_{OxA})^{-1}$ at high [PhOH] (Fig. 3b). The plateau suggests that, besides $OxA^{\bullet+}$, other intermediates that do not undergo back-reduction by PhOH are produced, differently from the previous case of degradation by ^{3}CBBP*.

Back reduction by PhOH has been observed for the degradation of anilines by $CO_3^{\bullet-}$, with $[\text{PhOH}]_{1/2}$ ~1–2 μM (Carena et al., 2022). In the present case, the irradiation experiments had to be carried out at pH 10 to ensure straightforward reaction pathways (**Text S3**), but in these conditions PhOH is ~50 % deprotonated to phenolate. Considering that phenolate is a stronger reducing agent compared to phenol (Arnold et al., 2017), a higher value of $[\text{PhOH}]_{1/2}$ would probably be expected at lower pH.

Degradation by direct photolysis. Variable concentrations of PhOH (0.5–10 μM) were added to solutions containing 6 μM OxA at pH 8.5, which were then irradiated under UVB light. The addition of PhOH inhibited the direct photolysis of OxA considerably (**Fig.S5c**), and the rate of direct photolysis (R^0_{OxA} without PhOH, R_{OxA} upon addition of PhOH) decreased with increasing [PhOH] down to a plateau (Fig. 3c).

UVB-light screening by PhOH can be ruled out by lack of absorption, and it is unlikely that PhOH acts by scavenging reactive species produced by irradiated OxA because the experimental data exclude an important role of self-sensitized OxA photolysis, which could be triggered by such species (see Section 3.1). Conversely, the experimental data of $R_{OxA} \cdot (R^0_{OxA})^{-1}$ *vs.* [PhOH] are well described by Eq. (3) (Fig. 3**c**). In this framework, it can be assumed that OxA undergoes direct photolysis and yields $OxA^{\bullet+}$ (with fraction f) plus other photoproducts (R.10), of which only $OxA^{\bullet+}$ undergoes back reduction (R.7).

$$\text{OxA} \xrightarrow{h\nu} \text{OxA}^{\bullet+} + \text{further products} \quad \text{(R.10)}$$

The numerical fit of the experimental data with Eq. (3) yielded $[\text{PhOH}]_{1/2} = (0.75 \pm 0.20)$ μM and $f = 0.76 \pm 0.05$, thereby suggesting that the antioxidant effect of PhOH was also effective for OxA direct photolysis.

The values of $[\text{PhOH}]_{1/2}$ observed for OxA direct photolysis and degradation by ^{3}CBBP* were quite similar, while lower $[\text{PhOH}]_{1/2}$ was

found for $CO_3^{\bullet-}$. However, in the latter case, the value of $[PhOH]_{1/2}$ would be kept low by partial deprotonation of phenol to phenolate.

For the anilines, it has been shown that $[PhOH]_{1/2}$ depends on the type of intermediate that is produced upon substrate oxidation by $^3CDOM^*/CO_3^{\bullet-}$ and that undergoes back reduction, rather than on the PPRI involved in the reaction that produces the given intermediate (Carena et al., 2022). This is reasonable, when considering that the value of $[PhOH]_{1/2}$ is determined by the competition between R.6 and R.7. Moreover, $^3CDOM^*$ and $CO_3^{\bullet-}$ react with contaminants through electron transfer reactions (energy-transfer reactions are additionally important for $^3CDOM^*$) (McNeill and Canonica, 2016; Wojnárovits et al., 2020), and the same reactions could be operational with OxA to produce $OxA^{\bullet+}$.

3.4. Modeling OxA photodegradation in surface waters

The obtained quantum yields of direct photolysis under UVB and UVA light and the bimolecular rate constants of OxA reactions with PPRIs (**Table S1**) were used to model photodegradation in surface waters with the APEX software (Lastre-Acosta et al., 2019). The different effects of (C)DOM on OxA photodegradation were taken into account (triplet sensitization, light screening, PPRI scavenging, and antioxidant effects; **Text S4**). In the case of the antioxidant effect, it should be considered that phenolic antioxidants in natural waters are part of the DOM, here quantified as Dissolved Organic Carbon, DOC. The experimental values of $[PhOH]_{1/2}$ (μM) were thus converted into $DOC_{1/2}$ ($mg_C\ L^{-1}$) as $DOC_{1/2} = 0.4 \cdot [PhOH]_{1/2}$ (Carena et al., 2022; Leresche et al., 2016).

In a 5 m-deep freshwater column, the photochemical half-life time of OxA ($t_{1/2}$) would be less than ten days for DOC ≤ 5 $mg_C\ L^{-1}$ (Fig. 4a), which is in agreement with the literature reports (Lai and Lin, 2009). In these conditions, OxA photodegradation by direct photolysis and $CO_3^{\bullet-}$ would prevail over the reactions with $HO^\bullet$ and $^3CDOM^*$. Photodegradation kinetics would also become slower ($t_{1/2}$ = 10–24 days) with increasing DOC up to 10 $mg_C\ L^{-1}$, in agreement with reported experimental data (Louros et al., 2020). The main effects of (C)DOM would be light screening (direct photolysis inhibition), $CO_3^{\bullet-}$ scavenging, and back reduction that inhibits both direct photolysis and degradation by $CO_3^{\bullet-}$ and $^3CDOM^*$.

In a 5 m-deep seawater column, OxA photodegradation would be very fast (lifetime of some hours) and dominated by reaction with $Br_2^{\bullet-}$ (Fig. 4b). However, the modeled process appears a bit too fast when compared with the available experimental data of OxA irradiation in seawater (Lunestad et al., 1995). $Br_2^{\bullet-}$ is a PPRI that mainly reacts with contaminants through electron transfer (Lei et al., 2021), in a comparable way as $^3CDOM^*$ and $CO_3^{\bullet-}$, thus a back-reduction effect might also affect the degradation of OxA by $Br_2^{\bullet-}$. Unfortunately, the value of $[PhOH]_{1/2}$ is unknown in the case of $Br_2^{\bullet-}$, due to the lack of an experimental protocol to quantify the back-reduction effect for $Br_2^{\bullet-}$-induced reactions. Further studies are required to fill this gap. Fig. 4c shows OxA photodegradation in seawater when a back-reduction effect on $Br_2^{\bullet-}$ is hypothesized, by assuming $DOC_{1/2}$ = 0.2 $mg_C\ L^{-1}$ (average of the $DOC_{1/2}$ values obtained for OxA direct photolysis and reactions with $^3CDOM^*/CO_3^{\bullet-}$). In this case, when considering the antioxidant effect on the $Br_2^{\bullet-}$ process, model results appear more reasonable (Lunestad et al., 1995). Interestingly, $t_{1/2}$ values in seawater would be lower, though still comparable, than those in freshwater and the $CO_3^{\bullet-}$ reaction would be largely replaced by $Br_2^{\bullet-}$. The formation of $CO_3^{\bullet-}$ in seawater is strongly inhibited by the efficient scavenging of $HO^\bullet$ by Br^- (Buxton et al., 1988).

Finally, the present model has some limitations. For instance, divalent cations may stabilize OxA by complexation and slow its direct photolysis in seawater (Louros et al., 2020). Additionally, $Cl_2^{\bullet-}$ may participate in OxA photodegradation in seawater, although $Cl_2^{\bullet-}$ concentrations are one/two-orders of magnitude lower than those of $Br_2^{\bullet-}$ (Vione et al., 2014). However, these processes must be investigated in detail and were not considered here.

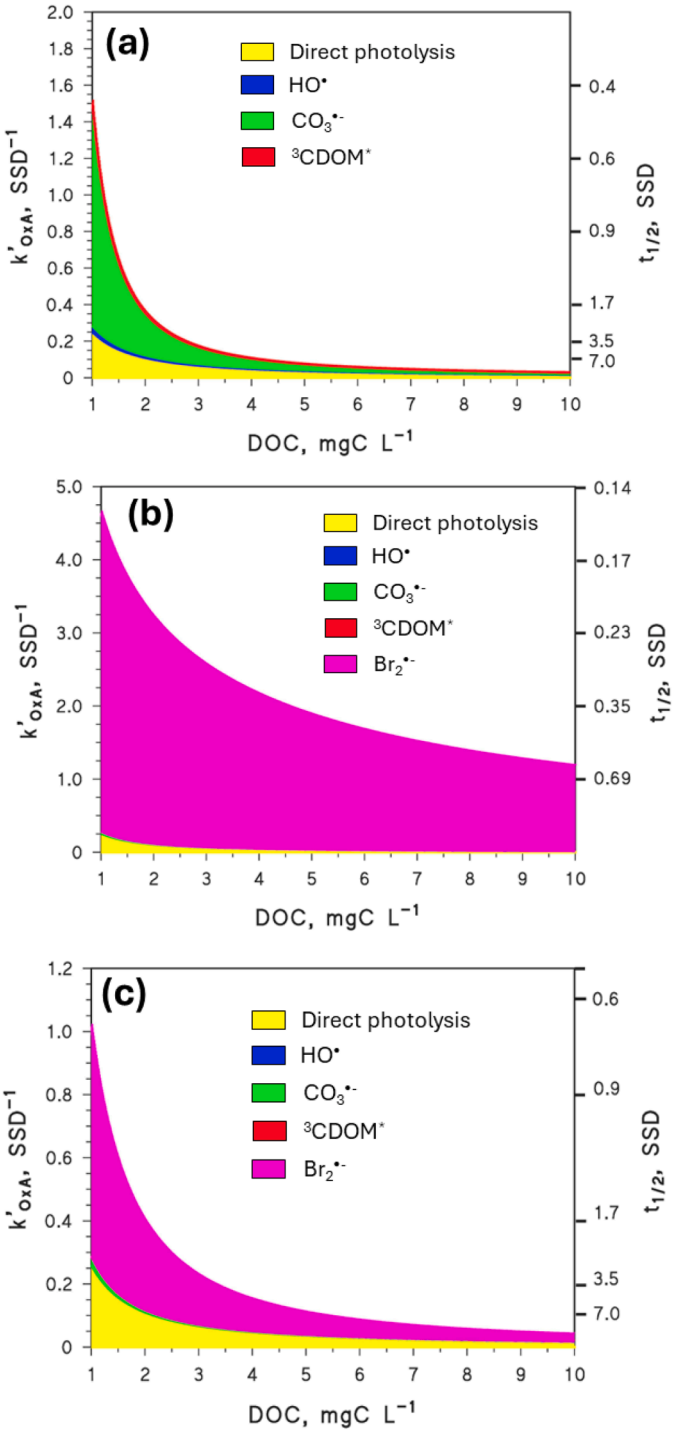

Fig. 4. Photodegradation rate coefficients and half-life times of OxA in **(a)** fresh- and **(b, c)** seawater (water depth d = 5 m). The contributions of direct photolysis and PPRIs are shown with different colors. In **(b)**, the photolysis of OxA induced by $Br_2^{\bullet-}$ was not considered to be affected by the antioxidant effect of DOM, while in **(c)** this inhibition pathway was considered. Other data about water chemical composition are the following: $1{\cdot}10^{-4}$ M NO_3^-, $1{\cdot}10^{-6}$ M NO_2^-, $1{\cdot}10^{-3}$ M HCO_3^-, $5{\cdot}10^{-6}$ M CO_3^{2-}, and pH 8 for freshwater; for seawater: $5{\cdot}10^{-6}$ M NO_3^-, $2{\cdot}10^{-7}$ M NO_2^-, $1{\cdot}10^{-3}$ M HCO_3^-, $5{\cdot}10^{-6}$ M CO_3^{2-}, $8.14{\cdot}10^{-4}$ M Br^-, and pH 8. SSD = summer sunny day equivalent to fair-weather 15 July at 45°N latitude.

4. Conclusions

- The anionic form of oxolinic acid showed significant photoreactivity by both direct and indirect photolysis, with bimolecular rate constants of the reactions with $HO^{\bullet}$ and $CO_3^{\bullet-}$radicals that approach the diffusion limit in water.
- As predicted by APEX, the direct photolysis and the reactions with $CO_3^{\bullet-}$ are key photodegradation pathways of OxA in freshwater, while the direct photolysis and the reactions with $Br_2^{\bullet-}$ are important in seawater. Overall, the antibiotic lifetime in mid-latitude summertime conditions is expected to be in the order of some days in both freshwater and shallow seawater (5 m water depth), where the anionic form of oxolinic acid prevails (pH > 7). Further studies will still be required to investigate the antibiotic photodegradation in conditions where the protonated form of oxolinic acid predominates (pH < 6).
- The photochemical degradation of OxA would be inhibited by (C)DOM, in agreement with literature reports, because of a combination of light screening, scavenging of PPRIs (especially $CO_3^{\bullet-}$ and $Br_2^{\bullet-}$), and antioxidant effects. The latter appear to be important whenever oxidation reactions by electron transfer are operational.

CRediT authorship contribution statement

Luca Carena: Writing – original draft, Methodology, Investigation, Funding acquisition, Formal analysis, Data curation, Conceptualization. **Silvia Bertolotti:** Writing – original draft, Investigation, Formal analysis, Data curation. **Viola Minutoli:** Writing – review & editing, Investigation, Formal analysis. **Mohamed Sarakha:** Writing – review & editing, Resources, Methodology, Data curation. **Annabel Fernandes:** Writing – review & editing, Investigation. **Ana Lopes:** Writing – review & editing, Funding acquisition. **Fabrizio Sordello:** Writing – review & editing, Formal analysis. **Marco Minella:** Writing – review & editing, Resources, Methodology. **Davide Vione:** Writing – review & editing, Software, Resources.

Declaration of competing interest

The authors declare that they have no known competing financial interests or personal relationships that could have appeared to influence the work reported in this paper.

Acknowledgements

This work was part of a project financed by the Grant for Internationalization - GFI of the University of Torino (CUP: D13C22001930001). LC, FS, MM and DV acknowledge support from the Project CH4.0 under the MUR program "Dipartimenti di Eccellenza 2023–2027″ (CUP: D13C22003520001). DV also acknowledges support from European Union – Next Generation EU, in the framework of the project GRINS - Growing Resilient, INclusive and Sustainable (PE00000018, CUP D13C22002160001). AF acknowledges Fundação para a Ciência e a Tecnologia (FCT) and Universidade da Beira Interior for the research contract CEECINST/00016/2021/CP2828/CT0006, under the scope of the CEEC Institutional 2021, funded by FCT.

Supplementary materials

Supplementary material associated with this article can be found, in the online version, at doi:10.1016/j.watres.2024.122880.

Data availability

Data will be made available on request.

References

Ahmad, A., Sheikh Abdullah, S.R., Hasan, H.A., Othman, A.R., Ismail, N.'Izzati, 2021. Aquaculture industry: supply and demand, best practices, effluent and its current issues and treatment technology. J. Environ. Manage. 287, 112271. https://doi.org/10.1016/j.jenvman.2021.112271.

Arnold, W.A., Oueis, Y., O'Connor, M., Rinaman, J.E., Taggart, M.G., McCarthy, R.E., Foster, K.A., Latch, D.E., 2017. QSARs for phenols and phenolates: oxidation potential as a predictor of reaction rate constants with photochemically produced oxidants. Environ. Sci. Process. Impacts 19, 324–338. https://doi.org/10.1039/c6em00580b.

Bedini, A., De Laurentiis, E., Sur, B., Maurino, V., Minero, C., Brigante, M., Mailhot, G., Vione, D., 2012. Phototransformation of anthraquinone-2-sulphonate in aqueous solution. Photochem. Photobiol. Sci. 11, 1445–1453. https://doi.org/10.1039/C2PP25111F.

Bhat, A.P., Pomerantz, W.C.K., Arnold, W.A., 2023. Wavelength-Dependent UV-LED photolysis of fluorinated pesticides and pharmaceuticals. Environ. Sci. Technol. 57, 5327–5336. https://doi.org/10.1021/acs.est.3c00627.

Bodrato, M., Vione, D., 2014. APEX (Aqueous photochemistry of environmentally occurring Xenobiotics): a free software tool to predict the kinetics of photochemical processes. Environ. Sci. Process. Impacts 16, 732–740. https://doi.org/10.1039/c3em00541k.

Brigante, M., Charbouillot, T., Vione, D., Mailhot, G., 2010. Photochemistry of 1-Nitronaphthalene: a potential source of singlet oxygen and radical species in atmospheric waters. J. Phys. Chem. A 114, 2830–2836. https://doi.org/10.1021/jp910203y.

Buxton, G.V., Greenstock, C.L., Helman, P.W., Ross, A.B., 1988. Critical review of rate constants for reactions of hydrated electrons, hydrogen atoms and hydroxyl radicals (·OH/·O−) in aqueous solution. J. Phys. Chem. Ref. Data 17, 513–886. https://doi.org/10.1063/1.555805.

Canonica, S., Hellrung, B., Wirz, J., 2000. Oxidation of phenols by triplet aromatic ketones in aqueous solution. J. Phys. Chem. A 104, 1226–1232. https://doi.org/10.1021/jp9930550.

Canonica, S., Laubscher, H.U., 2008. Inhibitory effect of dissolved organic matter on triplet-induced oxidation of aquatic contaminants. Photochem. Photobiol. Sci. 7, 547–551. https://doi.org/10.1039/b719982a.

Carena, L., Puscasu, C.G., Comis, S., Sarakha, M., Vione, D., 2019. Environmental photodegradation of emerging contaminants: a re-examination of the importance of triplet-sensitised processes, based on the use of 4-carboxybenzophenone as proxy for the chromophoric dissolved organic matter. Chemosphere 237, 124476. https://doi.org/10.1016/j.chemosphere.2019.124476.

Carena, L., Vione, D., Minella, M., Canonica, S., Schönenberger, U., 2022. Inhibition by phenolic antioxidants of the degradation of aromatic amines and sulfadiazine by the carbonate radical (CO3•−). Water Res 209, 117867. https://doi.org/10.1016/j.watres.2021.117867.

Choi, S., Sim, W., Jang, D., Yoon, Y., Ryu, J., Oh, J., Woo, J.-S., Kim, Y.M., Lee, Y., 2020. Antibiotics in coastal aquaculture waters: occurrence and elimination efficiency in oxidative water treatment processes. J. Hazard. Mater. 396, 122585. https://doi.org/10.1016/j.jhazmat.2020.122585.

Das, P.K., Encinas, M.V., Scaiano, J.C., 1981. Laser flash photolysis study of the reactions of carbonyl triplets with phenols and photochemistry of p-hydroxypropiophenone. J. Am. Chem. Soc. 103, 4154–4162. https://doi.org/10.1021/ja00404a029.

de la Casa-Resino, I., Empl, M.T., Villa, S., Kolar, B., Fabrega, J., Lillicrap, A.D., Karamanlis, X.N., Carapeto-García, R., 2021. Environmental risk assessment of veterinary medicinal products intended for use in aquaculture in Europe: the need for developing a harmonised approach. Environ. Sci. Eur. 33, 84. https://doi.org/10.1186/s12302-021-00509-8.

FAO, 2024. The State of World Fisheries and Aquaculture 2024. Blue Transformation in action, Rome. https://doi.org/10.4060/cd0683en.

Guo, Z., Wang, J., Chen, X., Cui, F., Wang, T., Zhou, C., Song, G., Zhang, S., Chen, J., 2021. Photochemistry of dissolved organic matter extracted from coastal seawater: excited triplet-states and contents of phenolic moieties. Water Res 188, 116568. https://doi.org/10.1016/j.watres.2020.116568.

Hopanna, M., Kelly, L., Blaney, L., 2020. Photochemistry of the organoselenium compound ebselen: direct photolysis and reaction with active intermediates of conventional reactive species sensitizers and quenchers. Environ. Sci. Technol. 54, 11271–11281. https://doi.org/10.1021/acs.est.0c03093.

Huang, K., Zhang, H., 2022. A comprehensive kinetic model for phenol oxidation in seven advanced oxidation processes and considering the effects of halides and carbonate. Water Res. X 14, 100129. https://doi.org/10.1016/j.wroa.2021.100129.

Janssen, E.M.-L., Erickson, P.R., McNeill, K., 2014. Dual roles of dissolved organic matter as sensitizer and quencher in the photooxidation of tryptophan. Environ. Sci. Technol. 48, 4916–4924. https://doi.org/10.1021/es500535a.

Lai, H.-T., Lin, J.-J., 2009. Degradation of oxolinic acid and flumequine in aquaculture pond waters and sediments. Chemosphere 75, 462–468. https://doi.org/10.1016/j.chemosphere.2008.12.060.

Lastre-Acosta, A.M., Barberato, B., Parizi, M.P.S., Teixeira, A.C.S.C., 2019. Direct and indirect photolysis of the antibiotic enoxacin: kinetics of oxidation by reactive photo-induced species and simulations. Environ. Sci. Pollut. Res. 26, 4337–4347. https://doi.org/10.1007/s11356-018-2555-4.

Le, T.X., Munekage, Y., Kato, S., 2005. Antibiotic resistance in bacteria from shrimp farming in mangrove areas. Sci. Total Environ. 349, 95–105. https://doi.org/10.1016/j.scitotenv.2005.01.006.

Lei, Y., Lei, X., Westerhoff, P., Tong, X., Ren, J., Zhou, Y., Cheng, S., Ouyang, G., Yang, X., 2022. Bromine radical (Br• and Br2•–) reactivity with dissolved organic matter and brominated organic byproduct formation. Environ. Sci. Technol. 56, 5189–5199. https://doi.org/10.1021/acs.est.2c00549.

Lei, Y., Lei, X., Yu, Y., Li, K., Li, Z., Cheng, S., Ouyang, G., Yang, X., 2021. Rate constants and mechanisms for reactions of bromine radicals with trace organic contaminants. Environ. Sci. Technol. 55, 10502–10513. https://doi.org/10.1021/acs.est.1c02313.

Leresche, F., Ludvíková, L., Heger, D., von Gunten, U., Canonica, S., 2020. Quenching of an aniline radical cation by dissolved organic matter and phenols: a laser flash photolysis study. Environ. Sci. Technol. 54, 15057–15065. https://doi.org/10.1021/acs.est.0c05230.

Leresche, F., Von Gunten, U., Canonica, S., 2016. Probing the photosensitizing and inhibitory effects of dissolved organic matter by using N,N-dimethyl-4-cyanoaniline (DMABN). Environ. Sci. Technol. 50, 10997–11007. https://doi.org/10.1021/acs.est.6b02868.

Lewis, K.A., Tzilivakis, J., Warner, D., Green, A., 2016. An international database for pesticide risk assessments and management. Hum. Ecol. Risk Assess. An Int. J. 22, 1050–1064. https://doi.org/10.1080/10807039.2015.1133242.

Louros, V.L.dos, Silva, C.P., Nadais, H., Otero, M., Esteves, V.I., Lima, D.L.D., 2020. Oxolinic acid in aquaculture waters: can natural attenuation through photodegradation decrease its concentration? Sci. Total Environ. 749, 141661. https://doi.org/10.1016/j.scitotenv.2020.141661.

Ludvíková, L., Friš, P., Heger, D., Šebej, P., Wirz, J., Klán, P., 2016. Photochemistry of rose bengal in water and acetonitrile: a comprehensive kinetic analysis. Phys. Chem. Chem. Phys. 18, 16266–16273. https://doi.org/10.1039/C6CP01710J.

Lulijwa, R., Rupia, E.J., Alfaro, A.C., 2020. Antibiotic use in aquaculture, policies and regulation, health and environmental risks: a review of the top 15 major producers. Rev. Aquac. 12, 640–663. https://doi.org/10.1111/raq.12344.

Lunestad, B.T., Samuelsen, O.B., Fjelde, S., Ervik, A., 1995. Photostability of eight antibacterial agents in seawater. Aquaculture 134, 217–225. https://doi.org/10.1016/0044-8486(95)00065-A.

Mack, J., Bolton, J.R., 1999. Photochemistry of nitrite and nitrate in aqueous solution: a review. J. Photochem. Photobiol. A Chem. 128, 1–13. https://doi.org/10.1016/S1010-6030(99)00155-0.

McNeill, K., Canonica, S., 2016. Triplet state dissolved organic matter in aquatic photochemistry: reaction mechanisms, substrate scope, and photophysical properties. Environ. Sci. Process. Impacts 18, 1381–1399. https://doi.org/10.1039/C6EM00408C.

Minella, M., Rapa, L., Carena, L., Pazzi, M., Maurino, V., Minero, C., Brigante, M., Vione, D., 2018. An experimental methodology to measure the reaction rate constants of processes sensitised by the triplet state of 4-carboxybenzophenone as a proxy of the triplet states of chromophoric dissolved organic matter, under steady-state irradiation conditions. Environ. Sci. Process. Impacts 20, 1007–1019. https://doi.org/10.1039/c8em00155c.

Nelson, N.B., Siegel, D.A., 2013. The global distribution and dynamics of chromophoric dissolved organic matter. Ann. Rev. Mar. Sci. 5, 447–476. https://doi.org/10.1146/annurev-marine-120710-100751.

Panthi, S., Sapkota, A.R., Raspanti, G., Allard, S.M., Bui, A., Craddock, H.A., Murray, R., Zhu, L., East, C., Handy, E., Callahan, M.T., Haymaker, J., Kulkarni, P., Anderson, B., Craighead, S., Gartley, S., Vanore, A., Betancourt, W.Q., Duncan, R., Foust, D., Sharma, M., Micallef, S.A., Gerba, C., Parveen, S., Hashem, F., May, E., Kniel, K., Pop, M., Ravishankar, S., Sapkota, A., 2019. Pharmaceuticals, herbicides, and disinfectants in agricultural water sources. Environ. Res. 174, 1–8. https://doi.org/10.1016/j.envres.2019.04.011.

Peng, Q., Song, J., Li, X., Yuan, H., Li, N., Duan, L., Zhang, Q., Liang, X., 2019. Biogeochemical characteristics and ecological risk assessment of pharmaceutically active compounds (PhACs) in the surface seawaters of Jiaozhou Bay, North China. Environ. Pollut. 255, 113247. https://doi.org/10.1016/j.envpol.2019.113247.

Pouliquen, H., Delépée, R., Larhantec-Verdier, M., Morvan, M.-L., Le Bris, H., 2007. Comparative hydrolysis and photolysis of four antibacterial agents (oxytetracycline oxolinic acid, flumequine and florfenicol) in deionised water, freshwater and seawater under abiotic conditions. Aquaculture 262, 23–28. https://doi.org/10.1016/j.aquaculture.2006.10.014.

Rigos, G., Nengas, I., Alexis, M., Troisi, G.M., 2004. Potential drug (oxytetracycline and oxolinic acid) pollution from Mediterranean sparid fish farms. Aquat. Toxicol. 69, 281–288. https://doi.org/10.1016/j.aquatox.2004.05.009.

Samuelsen, O.B., 2006. Pharmacokinetics of quinolones in fish: a review. Aquaculture 255, 55–75. https://doi.org/10.1016/j.aquaculture.2005.12.008.

Samuelsen, O.B., Lunestad, B.T., Husevåg, B., Hølleland, T., Ervik, A., 1992. Residues of oxolinic acid in wild fauna following medication in fish farms. Dis. Aquat. Organ. 12, 111–119. https://doi.org/10.3354/dao012111.

Shah, S.Q.A., Cabello, F.C., L'Abée-Lund, T.M., Tomova, A., Godfrey, H.P., Buschmann, A.H., Sørum, H., 2014. Antimicrobial resistance and antimicrobial resistance genes in marine bacteria from salmon aquaculture and non-aquaculture sites. Environ. Microbiol. 16, 1310–1320. https://doi.org/10.1111/1462-2920.12421.

Siedlewicz, G., Białk-Bielińska, A., Borecka, M., Winogradow, A., Stepnowski, P., Pazdro, K., 2018. Presence, concentrations and risk assessment of selected antibiotic residues in sediments and near-bottom waters collected from the Polish coastal zone in the southern Baltic Sea — summary of 3years of studies. Mar. Pollut. Bull. 129, 787–801. https://doi.org/10.1016/j.marpolbul.2017.10.075.

Tamtam, F., Mercier, F., Le Bot, B., Eurin, J., Tuc Dinh, Q., Clément, M., Chevreuil, M., 2008. Occurrence and fate of antibiotics in the Seine River in various hydrological conditions. Sci. Total Environ. 393, 84–95. https://doi.org/10.1016/j.scitotenv.2007.12.009.

Vione, D., Minella, M., Maurino, V., Minero, C., 2014. Indirect photochemistry in sunlit surface waters: photoinduced production of reactive transient species. Chem. Eur. J. 20, 10590–10606. https://doi.org/10.1002/chem.201400413.

Wenk, J., Canonica, S., 2012. Phenolic antioxidants inhibit the triplet-induced transformation of anilines and sulfonamide antibiotics in aqueous solution. Environ. Sci. Technol. 46, 5455–5462. https://doi.org/10.1021/es300485u.

Wenk, J., Von Gunten, U., Canonica, S., 2011. Effect of dissolved organic matter on the transformation of contaminants induced by excited triplet states and the hydroxyl radical. Environ. Sci. Technol. 45, 1334–1340. https://doi.org/10.1021/es202028w.

Westerhoff, P., Mezyk, S.P., Cooper, W.J., Minakata, D., 2007. Electron pulse radiolysis determination of hydroxyl radical rate constants with Suwannee river fulvic acid and other dissolved organic matter isolates. Environ. Sci. Technol. 41, 4640–4646. https://doi.org/10.1021/es062529n.

Wojnárovits, L., Tóth, T., Takács, E., 2020. Rate constants of carbonate radical anion reactions with molecules of environmental interest in aqueous solution : a review. Sci. Total Environ. 717, 137219. https://doi.org/10.1016/j.scitotenv.2020.137219.

Xie, X., Hu, Y., Cheng, H., 2016. Mechanism, kinetics, and pathways of self-sensitized sunlight photodegradation of phenylarsonic compounds. Water Res 96, 136–147. https://doi.org/10.1016/j.watres.2016.03.053.

Yan, S., Liu, Y., Lian, L., Li, R., Ma, J., Zhou, H., Song, W., 2019. Photochemical formation of carbonate radical and its reaction with dissolved organic matters. Water Res 161, 288–296. https://doi.org/10.1016/j.watres.2019.06.002.

Zeghioud, H., Kamagate, M., Coulibaly, L.S., Rtimi, S., Assadi, A.A., 2019. Photocatalytic degradation of binary and ternary mixtures of antibiotics: reactive species investigation in pilot scale. Chem. Eng. Res. Des. 144, 300–309. https://doi.org/10.1016/j.cherd.2019.02.015.

Zhang, L., Wei, H., Wang, C., Cheng, Y., Li, Y., Wang, Z., 2024. Distribution and ecological risk assessment of antibiotics in different freshwater aquaculture ponds in a typical agricultural plain, China. Chemosphere 361, 142498. https://doi.org/10.1016/j.chemosphere.2024.142498.

Zhang, Z., Xie, X., Yu, Z., Cheng, H., 2019. Influence of chemical speciation on photochemical transformation of three fluoroquinolones (FQs) in water: kinetics, mechanism, and toxicity of photolysis products. Water Res 148, 19–29. https://doi.org/10.1016/j.watres.2018.10.027.

Zhou, H., Yan, S., Lian, L., Song, W., 2019. Triplet-state photochemistry of dissolved organic matter: triplet-state energy distribution and surface electric charge conditions. Environ. Sci. Technol. 53, 2482–2490. https://doi.org/10.1021/acs.est.8b06574.